



**AIAA 96-2715**

**Ion Engine Service Life Validation  
by Analysis and Testing**

**John R. Brophy and James E. Polk  
Jet Propulsion Laboratory  
Pasadena CA 91109**

**Vincent K. Rawlin  
Lewis Research Center  
Cleveland, OH 44135**

**32nd AIAA/ASME/SAE/ASEE  
Joint Propulsion Conference and Exhibit  
July 1-3, 1996 / Lake Buena Vista, FL**

## Ion Engine Service Life Validation by Analysis and Testing

John R. Brophy and James E. Polk

*Jet Propulsion Laboratory*

*California Institute of Technology*

*Pasadena, California*

Vincent J. Rawlin

*National Aeronautics and Space Administration*

*Lewis Research Center*

*Cleveland, Ohio*

Assessment of the NSTAR ion engine service life is being accomplished through a combination of long duration testing and probabilistic analyses of the credible failure modes. A literature review that examined 65 ion engine endurance tests performed over the past 35 years was conducted to compile a list of possible ion engine failure modes. This review revealed 18 different failure modes which interrupted 19 of these 65 tests. Of these 18 failure modes only 4 are believed to be applicable to the NSTAR ion engine. Three other potential failure mechanisms were also identified for a total of seven credible damage accumulation failure modes for the NSTAR engine. Probabilistic techniques are being used by the NSTAR life validation activity to account for uncertainties in the engine independent operating parameters and in models of the wear out mechanisms so that the resulting engine service life is not penalized through the use of overly conservative deterministic analyses. Examples of probabilistic analyses applied to structural failure of the accelerator grid by charge exchange erosion and structural failure of the screen grid through erosion by discharge chamber ions reveals that neither of these failure mechanisms is likely to prevent the successful completion of the ongoing NSTAR 8,000 hr endurance test.

### Introduction

NASA is currently conducting a program called NSTAR (NASA Solar electric propulsion Technology Application Readiness) to validate xenon ion propulsion technology for use on planetary and commercial spacecraft. The three key objectives of this activity are:

1. Validate the service life capability of the NSTAR 30-cm ion engine.
2. Flight test the NSTAR ion propulsion system on the New Millennium DS-1 spacecraft [1].
3. Transfer ion propulsion technology from the government to industry and user organizations.

This paper describes the approach and current status of the activity to validate the NSTAR ion engine service life.

<sup>1</sup> Group Supervisor, Advanced Propulsion Technology Group, Member AIAA

<sup>2</sup> Technical Group Leader, Advanced Propulsion Technology, Member AIAA

<sup>3</sup> Aerospace Engineer, Member AIAA

### Ion Engine Failure Risk

Ion engine failures may be grouped into two types, event-consequent failures in which a component is overstressed to failure in a single event, and damage-accumulation failures in which the slow accumulation of damage or aging effects eventually result in component failure. An example of an event-consequent failure took place during the first NSTAR wear test. In this event a voltage level was inadvertently applied to the laboratory-style high voltage propellant isolator which exceeded its voltage rating resulting in failure of the isolator and interruption of the thruster wear test [2]. In establishing the NSTAR ion engine service life it is assumed that event-consequent failure modes have been eliminated through short-term testing, analysis and design experience so that any short-term normal or expected off-normal operating mode for the engine will not result in the failure of any engine component.

For damage-accumulation failure modes it is impractical to establish the engine useful service life through testing

alone [3]. This is a consequence of the low-thrust nature of ion propulsion which requires engine lifetimes of order 8,000 hours and the number of successful mission duration endurance tests which would have to be performed in order to establish a low failure risk. Poll [3] estimates that 69 non failure mission duration life tests would have to be conducted in order to have 50% confidence that the probability of failure is no larger than one in a hundred. Clearly, it is impractical to perform 69 tests of 8,000 hrs in duration. Indeed, the NSTAR program will conduct only three long-duration tests:

1. One test for the full design life of the engine (8,000 hrs at full power) using a Lewis Research Center (LRC) built thruster.
2. One test for 150% of the engine design life (equivalent of 12,000 hrs at full power) with a thruster built by the NSTAR thruster contractor, Hughes Electron Dynamics Division (HEDD).
3. One cycled endurance test consisting of 5000 on/off cycles over the full design life with an HEDD built thruster.

In addition, two shorter duration NSTAR wear tests have been completed, a 2,000-hr test [2] and a 1,000-hr test [1], both using LRC built thrusters.

Validation of the service life and failure risk for the NSTAR ion engine will be established through a combination of the information obtained in these long-duration tests together with probabilistic analyses of the principal engine failure modes. This combined approach is essential since the NSTAR program contains too few long duration tests to establish a low engine failure risk by testing alone. This is further complicated by the fact that all of the tests are different by design. They have different operating modes and durations designed to reveal unknown failure modes and characterize long-term engine performance. Even the thrusters themselves won't be identical for all of these tests since they are being built by different organizations, and design modifications (of non-critical components) are already being made by HEDD). Understanding and modeling the physics of the principal failure modes provides the foundation which ties these tests together to validate the engine service life. Without this understanding design modifications, such as those made following the 2,000-hr test [2,4], could invalidate prior testing in the establishment of the engine failure risk.

In addition, the NSTAR ion engine must be throttled over a 1 to 1 input power variation. Understanding of the processes involved in the principal failure modes greatly enhances what can be said about failure risk for operation at threshold conditions where significantly less long duration test experience will be obtained. Finally, it is expected that after the NSTAR technology is accepted for use on planetary spacecraft mission planners will push for higher thruster performance (thrust, Isp) and/or longer life. The

NSTAR service life validation activity will be useful in evaluating the extent to which the NSTAR thruster can be used beyond its current design capability.

In the establishment of engine failure risk through a combination of long duration testing and probabilistic physics of failure analyses the primary purposes of the long duration tests are to

1. Identify previously unknown failure modes, and provide information to eliminate analysis oversights or errors.
2. Characterize the parameters which drive the results of the analyses.
3. Characterize the engine performance as a function of time.

Indeed, the first NSTAR wear test [2] revealed a previously unknown failure mechanism (erosion of the outer edge of the cathode orifice plate and heater wire).

A literature review of ion engine endurance testing over the past 35 years was performed in order to establish a preliminary list of the expected principal failure modes for the NSTAR ion engine. The results of this review are summarized in the first part of this paper. Following the literature review the current list of principal failure modes for the NSTAR ion engine is presented and discussed. Finally, examples of the application of probabilistic risk assessment to three of these failure modes are presented.

### Historical Review of Ion Engine Life Testing

Very early in the development of ion engine technology attractive engine performance levels were achieved. The first references of broad beam, electron bombardment ion engines quote experimentally demonstrated performances levels as high as 70% efficiency at 5500 s Isp [5,6,7]. Since that time in the early 1960's the history of ion propulsion technology development has been largely focused in three areas: achieving efficient operation at progressively lower specific impulses, scaling to other engine sizes, and achieving adequate engine life.

In the two decades that followed, technologists led primarily by the Lewis Research Center, were widely successful in the first two areas. Today's ion engines are the most efficient electric propulsion devices in the optimum specific impulse range for solar powered planetary spacecraft (2500 to 3000 s<sub>p</sub>) and efficient electron bombardment ion engines have been successfully scaled an order of magnitude in diameter in both directions from Kaufman's original 10-cm diameter thruster. Electron bombardment ion engines ranging from 1.3-cm dia with an input power of 7 W to 150-cm dia at 130 kW have been built and tested representing an inextensible 18,000 to 1 ratio in input power [8,9].

Demonstrating a useful engine life with a low failure risk, however, has proved to be a much more difficult

problem. The earliest references on ion thruster technology recognized the importance of lifetime [10,11] and much of the technology work since then has been focused on achieving this goal. Table 1 summarizes 65 ion engine endurance tests covering 9 different thruster sizes (5,8,10,12,14,15,20,25 and 30 cm diameter), and five different propellants (Hg, Cs, Xe, Ar and Kr) found in the literature covering the 35 years since the operation of the first broad-beam, electron-bombardment ion engine at LeRC [12-53].

In general the story of the development of long-life ion engines over the past three decades is one characterized by a continual reduction in the voltages of thruster components subject to ion sputtering. The literature reveals a history of component technology improvements which enable efficient thruster operation at ever lower (in magnitude) accelerator grid voltages and discharge voltages. The NSTAR ion engine, with its 25 V discharge [4] and -180 V accelerator grid voltage [2] represents the culmination of this trend.

Such was the story for the past 30 years, the first six or seven years of ion engine technology development, however, told a different story. In this case the search for a long-lived cathode technology played a principal role. In 1964 the best cathodes, the so-called thick-oxide-layer cathodes, had a demonstrated lifetime in an ion engine of about 600 hours [54]. The advent of the orificed hollow cathode and its application to ion engines in the mid-1960's almost immediately eliminated the cathode as a life-limiting component. Rawlin and Keislake [55] describe cathode endurance tests which were initiated in 1967 and demonstrated 12,000-hrs of cathode operation. To be sure there have been numerous improvements to hollow cathodes since they were first introduced and exhaustive testing covering at least 3 orders of magnitude in emission current. But hollow cathodes which are protected from contamination have proved to be remarkably robust almost right from the start. Both cathodes on SERT II thruster #1 operated for more than 16,000 hours in space and the cathodes on thruster #2 for 18,000 hours [16]. Operation of all four SERT II cathodes was terminated only when the mercury propellant was exhausted [16]. Ground tests of hollow cathodes have demonstrated greater than 20,000 hours of operation on mercury [56] and xenon [57]. However, for cyclic operation cathode heater reliability is still an active area of research [58].

### Failure Modes

From the data in Table 1 a list of failure modes which have occurred during ion engine endurance testing was compiled. This list of 18 different observed failure modes is given in Table 2. In compiling this list a failure was defined as any event which either necessitated opening the vacuum chamber to fix or resulted in a loss of full operating

capability. Thus, the baffle delamination of Ref. 28 is counted as a failure even though the test was continued for another 11,000 hours after the baffle was replaced. Similarly, the inability to operate at a beam current of 1.5 A after 7300 hours in Ref. 37 because the discharge would go into "low-mode" is also counted as a failure.

Of the 65 tests in Table 1, 19 were interrupted by a failure of some kind and 46 were voluntarily terminated. The high fraction of voluntarily terminated tests is a result primarily of the relatively short duration of these endurance tests. Only 6 of these tests were for longer than the 8,000-hr service life validation goal for NSTAR.

**Table 2 Historically Observed Ion Engine Failure Modes**

No.	Description
1	Accelerator groove erosion from neutralizer ions [16,18,22].
2	Accelerator grid structural failure due to direct ion impingement from defocused beamlets caused by large metallic flakes on the screen grid [23,24,37].
3	Accel. grid structural failure due to charge-exchange ion erosion [52].
4	Grid shorting due to accel. grid material sputter-deposited on the screen grid and subsequent flaring [15,49].
5	Uncleatable grid short [16,49].
6	Severe grid arcing (new grids) [42].
7	Neutralizer degradation due to orifice plate erosion [41].
8	Neutralizer degradation due to orifice clogging [13,14].
9	Isolator braze joint [45].
10	Hg isolator vaporizer degradation or failure [19,42].
11	Isolator failure due to excessive voltage [2].
12	Graphite baffle delamination [28].
13	Baffle erosion resulting in discharge "low-mode" [36,37].
14	Cathode heater failure [13,14].
15	Main cathode erosion (orifice enlargement) [43].
16	Shorted cathode keeper wire inside the ground screen (degradation of wire insulation) [38].
17	Frozen Hg propellant feed line [12].
18	Catastrophic loss of vacuum [34].

Failure mode 1 from Table 2 is the familiar "groove" erosion which resulted in the in-flight failure of the SERT II thrusters. Reorienting the neutralizer away from the grids eliminated this failure mode in the early 1970's.

Structural failure of the accel. grid due to direct ion impingement from defocused beamlets caused by large flakes of material on the screen grid (failure mode 2) is still a viable failure mode. Sputter-containment mesh added to

discharge chamber surfaces subject to sputter deposition, however, is designed to limit the size of flakes that do form to a size that isn't harmful.

Accelerator grid structural failure due to charge-exchange ion erosion (mode 3) will eventually occur if the engine is operated for a sufficiently long time. This failure mode will be discussed in detail in the next section.

Mode 4, grid shorting due to accelerator grid material sputter-deposited on the screen grid and subsequent flaking is considered to still be a credible failure mode.

Unrecoverable grid shorts (mode 5) were responsible for the failure of the SERT-II thrusters in flight [10] and was the mechanism for the grid failure in the test-to-failure [19]. Several other tests in Table I had grid shorts presumably due to flakes of material between the grids. In those tests where this did not result in engine failure the grid shorts were cleaned by discharging a capacitor into the short vaporizing the flake of material. The NSTAR system for New Millennium will include a grid cleaning circuit.

One of the J-series 30-cm thruster endurance tests failed due to severe arcing between the grids (mode 6). Since these grids were new the failure is believed to be due to manufacturing difficulties. It is not clear, however, why this problem wasn't identified during thruster acceptance testing. Since the resolution of this problem is not clear, it's impossible to say that it won't happen again. It seems reasonable that careful acceptance testing should make it very unlikely.

Neutralizer degradation (mode 7) due to orifice plate erosion is still a possibility and care is being taken in the NSTAR program to make sure the neutralizer is operated in a manner which results in minimum orifice plate erosion. This is done operating the neutralizer with sufficient propellant flow that both the DC and AC neutralizer keeper voltage levels are low (less than 25 V and 5 V peak-to-peak, respectively).

Neutralizer degradation due to orifice clogging (mode 8) is not a likely failure mode provided xenon of adequate purity is delivered to the cathode.

The failure of the isolator braze joint (mode 9) is believed to be a result of a chemical reaction between liquid Hg and the braze material. This is not an issue for Xenon-fueled thrusters.

Of the 19 engine failures out of the 65 tests in Table I, 6 (or nearly 1/3) were related to the high voltage propellant isolators which separate the grounded propellant system from the high voltage engine. Most of these failures (4 of 6) were due to contamination of the outer surface of the isolator which increased its conductivity (mode 10). The increased conductivity resulted in F-R heating of the isolator and the adjacent mercury vaporizer. Eventually, more power is conducted to the vaporizer from this heating mechanism than is being added by the vaporizer heater. When this point is reached the mercury flow rate cannot be

controlled and the engine is considered to have failed. With Xenon propellant the high voltage isolators are still subject to surface contamination, but the lack of vaporizers for Xenon makes the engine much more tolerant of this contamination. Failure of the high voltage isolators due to surface contamination is considered unlikely for the NSTAR engine.

The cathode high voltage propellant isolator in the first NSTAR 2,000-hr test failed when excessive voltage was applied across it (mode 11). Failures of this sort should not occur in future NSTAR testing since the high voltage power supplies to be used have a voltage capability that is less than the voltage rating of the isolators.

Baffles do not exist in the NSTAR imp-cusp discharge chamber configuration so failure mode 12 is not relevant to the NSTAR engine.

In the 10,000-hr test of Ref. 37, the baffle of the 30-cm divergent field thruster was so severely eroded after 7300 hrs that the discharge chamber would no longer function properly (mode 13). This produced a change in control characteristic in which the discharge chamber would only operate in "low-mode" characterized by low beam current, high main propellant flow rate and poor engine performance. Normal discharge chamber operation could be maintained only for beam currents below a certain level. The maximum achievable beam current decreased with time after 7300 hrs. The NSTAR thruster has no baffle and cathode pole piece and the main propellant flow rate is not controlled by the beam current so this exact failure mode can not occur in the NSTAR engine. However, it is possible that erosion or aging effects could degrade the discharge chamber performance to the point that the engine can no longer be operated at desired levels. Only the execution of the planned long-duration tests for NSTAR can determine if this is likely.

Cathode heater failure (mode 14) is still a viable failure mechanism, especially for missions in which thousands of on/off cycles are required. However, new heater materials developed for the Space Station Alpha plasma contactor have been successfully tested in excess of 10,000 on/off cycles [58].

Engine degradation due to enlargement of the main cathode orifice (mode 15) has not been observed in the NSTAR thruster and it is believed that maintaining sufficient flow rate through the cathode and operating at low discharge voltages makes this an unlikely failure mechanism.

The test in Ref. 38 was halted by the cathode keeper wire which shorted to the thruster body preventing the cathode from starting (mode 16). The short occurred because the wire insulation degraded thermally. The NSTAR thruster is being designed to make sure the wire insulation has the appropriate temperature capability for the environment in which it will be used, so this failure mechanism, while possible, is considered unlikely.

Reference 12 lists a test of a mercury thruster which was interrupted when a mercury feed line froze and ruptured

during a period when the thruster was off (mode 17). The switch to xenon propellant eliminates this as a viable failure mode.

Finally, the test in Ref. 34 was halted by a catastrophic loss of vacuum while the engine was operating (mode 18). While this failure is not related to the thruster it is a possibility in any long duration test, although it is considered unlikely. Much of the information regarding erosion and sputter-deposition from this test was lost due to this event which resulted in significant oil back-streaming from the hot diffusion pumps onto the hot engine.

### **NSTAR Failure Modes**

Based on the above list of observed failures, extrapolation of the erosion characteristics from endurance tests which were suspended before failure, and testing experience with the NSTAR thruster the following list of credible failure modes for the NSTAR engine has been compiled.

1. Accelerator grid structural failure due to direct ion impingement from defocused beamlets caused by flakes on the screen grid.
2. Grid shorting by flakes too big to be cleared by the NSTAR grid clearing circuit.
3. Accelerator grid structural failure due to charge-exchange ion erosion.
4. Electron-backstreaming due to enlargement of the accelerator grid apertures.
5. Cathode heater failure due to thermal cycling.
6. Cathode orifice plate erosion.
7. Screen grid erosion.

Note, that failure modes 4, 6 and 7 in the above list did not appear in the list of 18 failure modes observed in previous ion engine endurance test experience. NSTAR failure mode 4, electron-backstreaming due to enlargement of the accelerator grid apertures was identified as a possible failure mechanism as a result of the 2,000- and 1,000-hr NSTAR wear tests [2,4]. Mode 6, cathode orifice plate erosion was also identified after the 2,000-hr test. Design changes made after the 2,000-hr test and preliminarily verified in the subsequent 1,000-hr test are believed to have significantly mitigated this failure mode [4].

Screen grid erosion (NSTAR failure mode 7) has been on the list of possible failure modes for ion engines for a long time. Severe screen grid erosion was observed in the 2,000-hr test. Design changes to reduce the fraction of doubly-charged ions in the discharge chamber and lower the voltage difference between the screen grid and the discharge chamber plasma made after this test resulted in very little screen grid erosion in the follow-on 1,000-hr test [4].

Failure mode 1 is a consequence of the production of sputter-deposited material in the discharge chamber which then flakes off and rests on the screen grid. In space, the

spacecraft acceleration due to propulsion system operation will tend to accelerate any loose flakes in the discharge chamber toward the screen grid. There are two approaches to reducing the risk of failures from this mechanism. The first and best way is to reduce the quantity of sputter-deposited material produced in the discharge chamber. The very low operating discharge voltage (25 V) and acceptable fraction of doubly-charged ions are intended to produce a very low screen grid erosion rate and since the screen grid is the primary source of sputtered material for the NSTAR thruster this should significantly reduce the risk of flake formation. The second approach is to treat the interior discharge chamber surfaces subject to net material deposition to make the deposited material adhere better and to control the size of any flakes which may be produced.

Failure mode 2 is also related to the production of metallic flakes from sputter-deposited material. In this case, however, the flakes could originate either from inside the discharge chamber or from accelerator grid material that is sputter-deposited on the screen grid.

Failure mode 3, as mentioned above, will eventually cause the engine to fail. Probabilistic modeling of this wear-out mode is presented in the following section to assess the failure risk from this mode for the NSTAR design life (qualification time of 12,000-hrs at full power).

Lastly, cathode heater failure due thermal cycling is primarily a materials issue. It is believed that heater testing being conducted in support of the space station plasma contactor program is directly applicable to the NSTAR thruster cathodes. Therefore, extensive heater thermal cycling tests are not included in the NSTAR life validation program with the exception that the third NSTAR long duration test is a cycling test in which the thruster will be subjected to 5,000 on/off cycles while demonstrating its full total impulse capability.

### **Probabilistic Risk Assessment**

#### **Sensitivity Testing**

The NSTAR ion engine operating point is determined by the values of five independent parameters: the main propellant flow rate, the cathode flow rate (the neutralizer flow rate is maintained equal to the cathode flow rate), the beam power supply voltage, the beam current, and the neutralizer keeper current. All other engine operating parameters such as thrust, Isp, input power, efficiency, discharge current, etc., are dependent parameters. At each point in the 4.6 to 1 input power throttle range of the NSTAR thruster the operating characteristics are determined by the values of the five independent parameters. These parameters, however, cannot be specified exactly. The uncertainties in these parameters for the NSTAR propulsion system are given in Table 3. The NSTAR propellant feed

system, for example, is being designed to control the propellant flow rates to  $\pm 3\%$ .

**Table 3 NSTAR Independent Parameter Uncertainties**

Independent Parameter	Uncertainty
Main Flow Rate	$\pm 3\%$
Cathode Flow Rate	$\pm 3\%$
Beam Current	$\pm 1\%$
Beam Power Supply Voltage	$\pm 5\%$
Neut. Keeper Current	$\pm 1\%$

A series of sensitivity tests was been conducted on the NSTAR engineering model thruster (EMT2) at both the Lewis Research Center and JPL. These tests were conducted using a Taguchi [61] experimental design approach to determine the sensitivity of the dependent parameters to variations in the independent parameters over the uncertainty ranges specified in Table 3. In the setup and conduct of these tests the effect of the neutralizer keeper current variations were ignored on the basis that this parameter has essentially no effect on the rest of the engine operation. The sensitivity data were then curve fit using commercially available software designed for this purpose [62]. The resulting curve fits are used to interpolate between the sensitivity test data points.

A Monte Carlo simulation was used to generate probability distribution functions for selected dependent parameters. This was done by assuming uniform distribution functions over their respective uncertainty ranges for all of the independent parameters. For a given trial a value for each independent parameter was randomly selected from within its distribution, and the value of the desired dependent parameter was calculated from the curve fits to the sensitivity data. This process was repeated for typically 30,000 trials. The results were tabulated and sorted into bins of uniform width covering the range of observed values for the selected dependent parameter. Typically 50 bins were used. Dividing the frequency of occurrence by the total number of trials gives the relative probability of observing the dependent parameter within a given bin.

The results of this procedure for the specific impulse at full power are given in Fig. 1, where each data symbol represents the value for a particular bin. This distribution in specific impulse is a result of the allowable variations in propellant flow rate, beam voltage and beam current, and has a standard deviation of 66 s. The other thruster parameters, thrust, efficiency, etc., have similar distributions.

In modeling certain wear-out modes it is of particular interest to know the behavior of the discharge voltage and the ratio of doubly charged ions in the discharge chamber. Following the procedure discussed above the full power distributions of both of these parameters were calculated and are shown in Figs. 2 and 3. The fact the independent engine

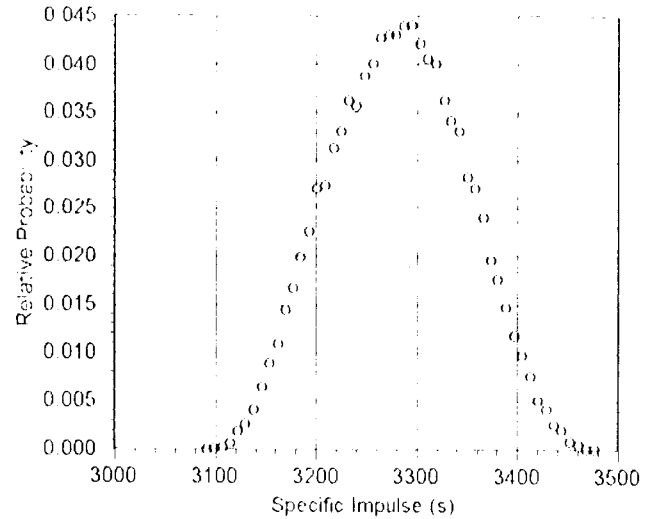


**Fig. 1 Specific impulse distribution based on sensitivity test results for operation at the NSTAR full power point.**

parameters cannot be controlled exactly has a direct impact on the modeling of engine wear-out modes and dictates that the wear-out mechanisms cannot be modeled deterministically. One could always select the worst case values from these distributions and use them in deterministic calculations of end of life, but doing so would artificially penalize the engine capability.

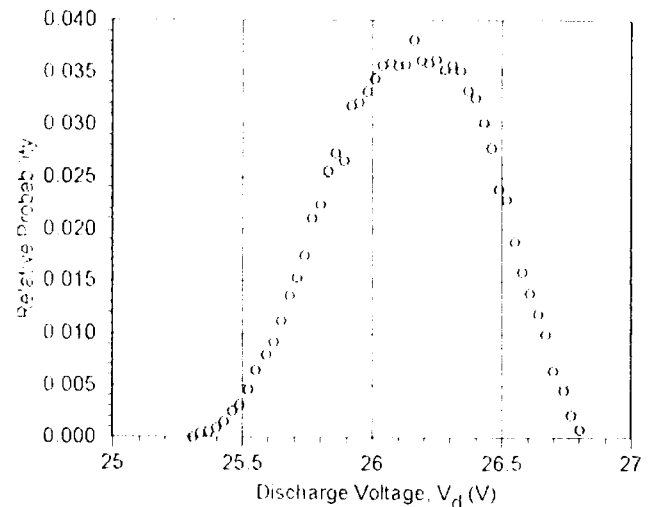


**Fig. 2 Discharge voltage distribution function at the NSTAR full power operating point.**

Probabilistic modeling techniques are better suited to situations such as this where the values of the inputs parameters are uncertain. In addition, we shall see that not

only are the operating conditions subject to uncertainties, but also that certain aspects of the wear-out models are also uncertain. The probabilistic methodology of Moore, et al. [63,64] enables both of these types of uncertainties to be treated in a quantifiable manner.

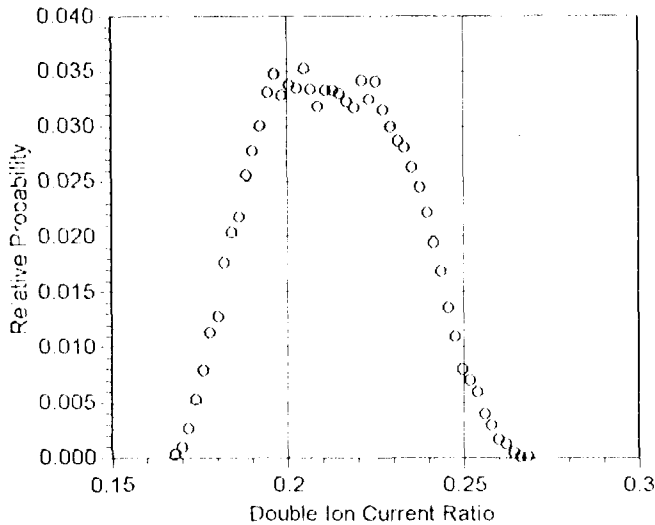


Fig. 3 Double ion current ratio distribution function at the NSTAR full power point.

#### Accelerator Grid Erosion – Structural Failure

One of the failure modes for ion engines is structural failure of the accelerator grid due to charge-exchange ion sputtering. Details of the accelerator grid charge-exchange erosion geometry have been described in detail by Polk [59] and Rawlin [60]. In general the accelerator grid fails structurally when the charge-exchange “pits and grooves” wear completely through the grid. It is expected that this will take place first at the center of the grid where the highest erosion rates are observed.

The total mass removed from the downstream face of the accelerator grid at the time of structural failure may be estimated by assuming the charge-exchange erosion remains entirely within the pit and grooves pattern. This is only approximately correct [19] since significant undercutting occurs on the upstream side of the accelerator grid near structural failure which is outside of the pits and grooves pattern [59]. The effect of this undercutting has been neglected in the analyses that follow making the results conservative. Assuming a rectangular cross section for the groove shape, the total mass removed from the accelerator grid at failure,  $m_f$ , is given by [59]

$$m_f = A_b(1 - \phi_a)\alpha f_a \rho t_a \quad (1)$$

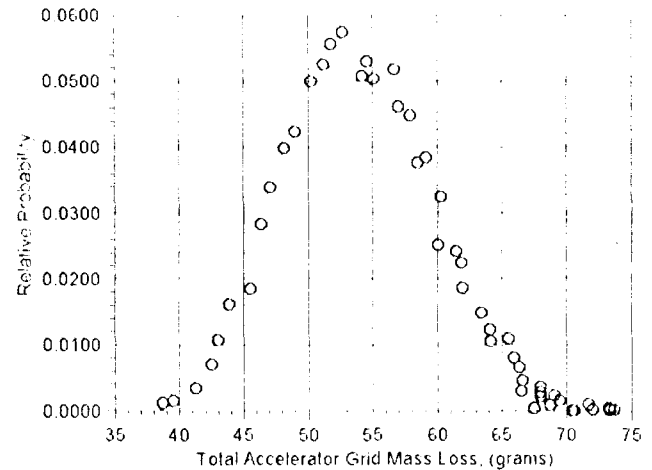


Fig. 4 Calculated probability distribution of accelerator grid mass loss at structural failure due to charge-exchange erosion.

where  $A_b$  is the active grid area,  $\phi_a$  is the initial accelerator grid open area fraction,  $\alpha$  is the fraction of the accelerator grid webbing covered by the pit and grooves erosion pattern,  $f_a$  is accelerator grid mass loss flatness parameter defined as the ratio of peak to average accelerator grid mass loss per unit area,  $\rho$  is the density of the grid material, and  $t_a$  is the accelerator grid thickness. The accelerator grid mass loss flatness parameter is assumed to be equal to the accelerator grid ion impingement current flatness parameter so that,

$$f_a = \frac{J_a}{A_b(1 - \phi_a)j_{a,cat}} \quad (2)$$

where  $J_a$  is the accelerator grid impingement current and  $j_{a,cat}$  the maximum accelerator grid impingement current density at the center of the grid averaged over the local pits and grooves erosion pattern.

The values of  $\alpha$  and  $f_a$  in Eq. (1) can not be specified exactly. This is a result primarily of a lack of knowledge about their true values and what the functional dependence of these parameters is on the thruster operating conditions. Based on measurements of the ion beam current density distribution across the grids of the NSTAR engine and empirical evidence that the accelerator grid mass loss distribution may be broader than the ion beam current distribution,  $f_a$  is assumed to be in the range 0.41 to 0.50. The eroded area fraction,  $\alpha$ , is approximated from photographs taken of the accelerator grids after the 2,000-hr and 1,000-hr tests [2,4] and is believed to be in the range 0.37 to 0.46. Based on these uncertainties Eq. (1) may be used to calculate the probability distribution of accelerator grid mass loss at failure. This distribution is shown in Fig. 4

for the parameter values given in Table 4. The accelerator grid mass loss at failure can, at best, be specified as a distribution rather than a single number because the inputs to Eq. (1) can not be specified exactly. The large range of possible values for the accelerator grid mass loss at failure reflects our lack of knowledge concerning the final grid erosion geometry.

**Table 4** Input parameter values for accelerator grid charge-exchange erosion model.

Parameter	Range of Values (uniform distributions)
Beam current, $I_b$ (A)	1.74 to 1.78
Beam power supply voltage (V)	1045 to 1155
Main flow rate (scem)	22.6 to 24.0
Cathode flow rate (scem)	2.91 to 3.09
$I_a/I_b$ (%)	0.35 to 0.50
$V_a$ (V)	171 to 189
$V_g$ (V)	11 to 15
$V_{fg}$ (V)	4 to 10
Mass loss flatness parameter, $f_a$	0.11 to 0.61
Eroded area fraction, $\alpha$	0.35 to 0.48
Effective sputter yield factor, $Z_0$	0.37 to 0.50

The rate at which accelerator grid mass is removed by charge-exchange ions,  $\dot{m}_g$ , is given by

$$\dot{m}_g = J_s \beta I \lambda_e \frac{m_i}{e} \quad (3)$$

where  $J$  is the sputter yield at normal incidence for xenon on molybdenum,  $\beta$  is the fraction of the measured accelerator grid current which strikes the pits and grooves erosion pattern on the downstream grid surface,  $m_i$  is the mass of an atom of grid material,  $e$  is the electron charge, and  $Z_0$  is a parameter which reflects the experimental observation that the net sputter yield for accelerator grids is only a fraction of the sputter yield at normal incidence. This is most likely due to redeposition effects in the pits and grooves due the relatively deep aspect ratio of these features or a lower average ion energy due to the production of significant numbers of charge-exchange ions in locations where the local potential is negative with respect to the beam plasma. The sputter yield information required by Eq. (3) was calculated from a curve fit to the data of Rosenberg and Welner [65].

The range for the ratio of accelerator current to beam current in Table 4 of 0.35 to 0.50 % was selected to capture the expected value in space at the low end to approximately the highest value observed during extended duration testing. The range for the coupling voltage,  $V_{fg}$  of 11 + 2 V was made

broad enough to capture existing data with about a 1 V margin on either side. The parameter  $V_g$  represents the potential of the beam plasma relative to the ambient space plasma (if in space) or facility ground for ground tests. Measurements at JPL with the NSTAR thruster indicate a value of 4 V for this parameter. Similar measurements on a 30-cm divergent field thruster in the NSTAR endurance test chamber returned a value of about 12 V. The SERT II flight data indicated that the beam plasma could be 30 to 40 V above the ambient space potential. Under these conditions the charge-exchange ions striking the screen grid would be expected to do so with an addition 30 or 40 eV. This is a small effect for the SERT II thrusters in which the accelerator grid voltage was -1600 V, but it is a significant fraction of the NSTAR accelerator grid voltage of -180 V. For the analyses herein,  $V_g$  was assumed to be in the range 4 to 10 V until this issue is better understood. Expanding the high end of this range to 40 V reduces the calculated grid life at a failure risk of 9.1 by approximately 2-khrs. The energy of the ions striking the downstream surface of the accelerator grid is given by  $T_{d1} + T_g + T_{fg}$ .

The mass loss flatness parameter,  $f_a$ , has a range of values determined by the measured ion beam current density flatness parameter at the low end, and the measured accelerator grid flatness parameter from the test of Ref. 47 at the high end. These data are believed to capture the actual value of  $f_a$  since there is evidence that the facility background pressure broadens  $f_a$  relative to the beam current density distribution and the NSTAR tests are performed at lower chamber pressures than the test of Ref. 47.

The range of possible values for the eroded area fraction given Table 4 represents the approximate measured value for  $\alpha$  from the 2,000-hr and 1,000-hr endurance tests at the low end and a value which encompasses the test of Ref. 47 at the high end [59].

The effective sputter yield variation in Table 4 covers the ratio of actual to calculated values from the NSTAR 1,000-hr test at the low end to the value 0.5 which has been observed in other ion engine endurance tests.

For the range of the input parameters given in Table 4 the distribution in accelerator grid mass loss rate due to charge-exchange ion sputtering was calculated and is shown in Fig. 5. In generating this distribution it was assumed that 75% of the accelerator grid impingement current strikes the pits and grooves pattern, i.e.,  $\beta = 0.75$ . In the 1,000-hr test [4] the accelerator grid mass loss rate in the pits and grooves was estimated to be 2.5 g/khr (after adjusting the measured mass change of the grid for sputter-deposited from the facility and for the mass lost in the enlargement of the accelerator grid apertures which suggests that  $\beta = 0.75$  may be about right). It should be noted however, that in the 2,000-hr test [2], the accelerator grid mass loss rate was much lower at about 1.3 g/khr. The reason for this large

difference is unknown given that the accelerator grid currents and voltages in these tests were nearly identical [4]

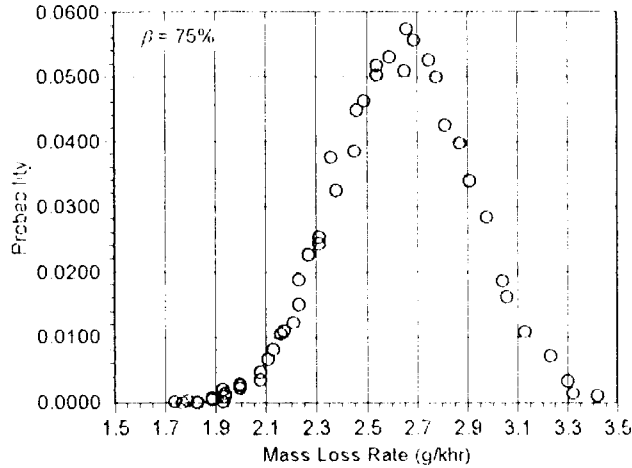


Fig. 5 Calculated distribution in accelerator grid mass loss rate due to charge-exchange ions, for operation at full power, assuming 75% of the accelerator grid current strikes the pits and grooves.

The time required to erode the accelerator grid to structural failure,  $T_f$ , may be obtained by combining Eqs. (1) and (3) to get

$$T_f = \frac{A_b(1 - \phi_a)\alpha f_a e \rho_a}{J_a \beta \gamma \lambda_y m_g} \quad (4)$$

It is clear from Figs. 4 and 5 that both the amount of mass removed by the time of failure and the rate at which it is removed are characterized by distributions. These distributions combine to produce a distribution in the calculated time to structural failure of the accelerator grid. Three such distributions have been calculated for three values of  $\beta = (0.60, 0.75, 0.90)$  and the range of parameters given in Table 4. Normalizing and then integrating these distributions over different run times results in curves of the probability of failure versus run time as shown in Fig. 6. For  $\beta = 0.75$ , the 50% conditional failure risk occurs at a run time of about 21,000 hours. For this curve there is no significant risk of failing the planned 8,000-hr endurance test due structural failure of the accelerator grid by charge-exchange erosion.

#### Screen Grid Erosion – Structural Failure

A second failure mode is sputter-erosion of the screen grid by ions produced in the discharge chamber. These are ions which are directed toward the accelerator system but

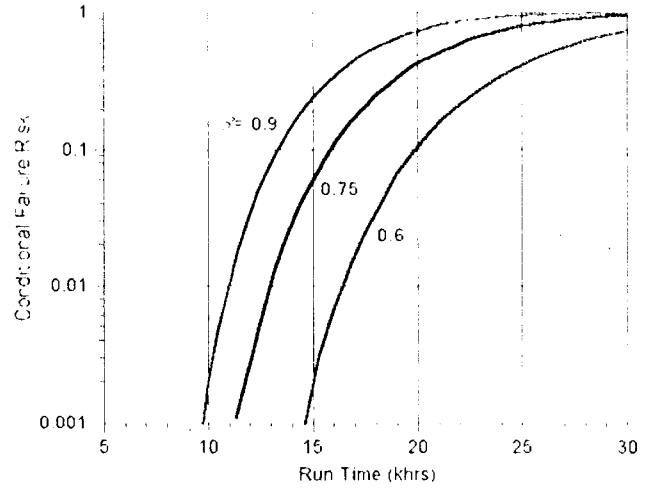


Fig. 6 Failure risk for the accelerator grid due structural failure from charge-exchange erosion at full power,  $\beta$  is the fraction of the accelerator grid current which causes the erosion on the downstream surface of the grid.

don't get focused through the screen grid apertures. Instead, they strike the screen grid webbing slowly reducing its thickness through sputtering. When the thickness of center region of the screen grid is reduced to zero the screen grid has failed.

The maximum rate at which the thickness of the screen grid is reduced is given by [66]

$$w = (j_s Y_s + \frac{j_{s+}}{2} Y_{s+}) \frac{m}{e \rho} \quad (5)$$

where  $w$  is the maximum screen grid thickness reduction rate,  $j_s$  and  $j_{s+}$  are the centerline singly-charged and doubly-charged ion current densities, respectively, and  $Y_s$  and  $Y_{s+}$  are the corresponding normal-incident sputter yields. The local ion current densities are related to the beam current by

$$j_s = \frac{1 - \phi_s}{\phi_s} \frac{j_b}{f_s A_b \phi_s (1 + f_s R_s^{1+})} \quad (6)$$

where  $\phi_s$  is the effective screen grid transparency to ions,  $\phi_s$  is the physical open area fraction of the screen grid,  $R_s^{1+}$  is the measured double to single ion current ratio, and  $f_s$  is a parameter which corrects the measured value of  $R_s^{1+}$  to its maximum centerline value [66], i.e.,

$$\frac{j_{s+}}{j_s} = f_s R_s^{1+} \quad (7)$$

The value of  $f_d$  was calculated by Rawlin [66] based on characteristics of the ExB probe used to measure  $R_1^{**}$  and more spatially detailed double ion data obtained on 30-cm mercury thrusters. The ExB probe was positioned far enough from the thruster that it would accept ions across the full thruster diameter in one axis. Thus, the probe measures essentially a double ion current ratio averaged along a diameter. The model of screen grid erosion, however, requires the value of the double ion current ratio on the centerline of the thruster. Therefore, Rawlin calculated a value for  $f_d$  to adjust the measured double ion current ratio to represent the centerline value. Rawlin's value was subsequently modified to account for the differences in ion beam flatness parameters between the NSTAR thruster and the mercury thrusters. This process produced the range of values for this parameter given in Table 5.

Combining Eqs. (5) and (6) results in the following expression for the maximum screen grid thickness reduction rate in terms of the independent and dependent parameters measured in the sensitivity tests.

$$w = \frac{1 - \phi_s}{\phi_s} \frac{J_s m_s \left( Y_1 + \frac{f_d}{2} R_1^{**} Y_{11} \right)}{f_d A_s (1 - \phi_s) e \rho (1 + f_d R_1^{**})} \quad (8)$$

End of life for the screen grid,  $T_{eg}$ , was determined by the time it took to erode completely through the grid at the rate given in Eq. (9), i.e.,

$$T_{eg} = \frac{t}{w} \quad (9)$$

Equation (8) requires the sputter yields for xenon incident on molybdenum at energies corresponding to the engine discharge voltage (of order 25 V). Unfortunately there is no sputter yield data at these voltages. Rawlin [66], therefore, extrapolated existing data into the required energy range using a threshold value of zero at an ion energy of 24.8 eV. Since extrapolations are inherently uncertain, an uncertainty of  $\pm 25\%$  was added to the sputter yield values calculated from this procedure.

The ion current flatness parameter,  $f_b$ , given in Table 5 is given a relatively narrow range from 0.4 to 0.44. This is a reflection that the beam current density distribution just downstream of the accelerator grid is measured directly and these measurements are believed to be a good representation of the ion current distribution to the screen grid inside the discharge chamber.

As in the accelerator grid erosion model a Monte Carlo simulation was performed using Eqs. (8) and (9) with the

ranges of input parameters specified in Table 5. The simulation consisted of 30,000 trials and produced the failure risk versus run time curve shown in Fig. 7. Clearly, these calculations indicated by the curve for operation at the nominal NSTAR full power point suggest a negligible failure risk in 8,000 or 12,000 hours due to screen grid erosion.

**Table 5 Input parameter values for the screen grid erosion model.**

Parameter	Range of Values (uniform distributions)
Beam current, $J_s$ (A)	1.74 to 1.78
Beam power supply voltage (V)	10.15 to 11.55
Main flow rate (scem)	22.6 to 24.0
Cathode flow rate (scem)	2.91 to 3.09
Accelerator grid voltage, $V_a$ (V)	171 to 189
Single ion sputter yield, $Y_1$	$\pm 25\%$
Double ion sputter yield, $Y_{11}$	$\pm 25\%$
Double ion ratio correction to centerline parameter, $f_d$	1.50 to 1.67
Ion current flatness parameter, $f_b$	0.4 to 0.44

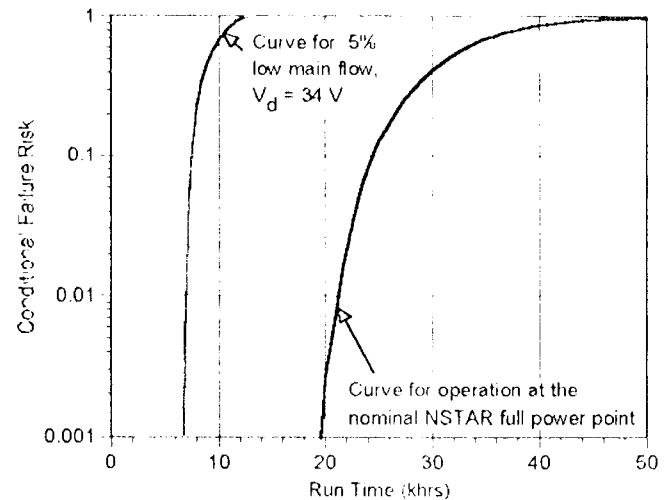


**Fig. 7 Calculated screen grid failure risk due to structural failure from sputtering.**

The other curve in Fig. 7 was generated by modifying the inputs used to generate the nominal full power case in three ways. First, the cathode flow rate was fixed at the nominal run flow rate (middle of the distribution). Second, the main flow rate was set to a fixed value 5% below the nominal main flow rate. Third, the discharge voltage was set to a fixed value of 34 V. These conditions were set to approximate the engine operating conditions believed to exist during the 2,000-hr test [2]. The curves in Fig. 8

indicate that the effect of these changes on the screen grid life is substantial. Under these conditions the 50% failure probability occurs at a run time of about 9,100-hrs. Linearly extrapolating the screen grid wear rate of  $47 \pm 2 \mu\text{m}/\text{km/hr}$  from the 2,000-hr test [2] indicates wear through of the 380  $\mu\text{m}$  thick grid in 7,800 to 8,400 hrs.

### Future Plans

Near-term future activities include refinements of the accelerator grid structural failure model. In particular the expected beam plasma potential in space is not well understood. A beam potential that is significantly higher (i.e. 10's of volts) than that assumed in the present analysis would significantly aggravate accelerator grid erosion.

Work is currently underway to develop a model of the erosion of the accelerator grid hole diameters and engine failure due to electron-backstreaming. It is possible that this may be the first failure mechanism for the thruster.

In addition, work is needed on modeling of the behavior of sputter-deposited films. A description of the activities which should be included in such a study are outlined by Polk [3]. This is important since historically a number of the observed failures have resulted from the formation of flakes in the discharge chamber.

Finally, mechanism which caused the high orifice plate erosion in the NSTAR 2,000-hr test is not understood, nor is the process by which this erosion mechanism was mitigated in the NSTAR 1,000-hr test understood. It is important to understand this mechanism in order to make sure we can avoid it in the future.

### Conclusions

A review of ion engine endurance testing over the past 35 years revealed 18 failure different mechanisms which interrupted 19 of the 65 extended duration tests conducted over this time period. Of these only four are believed to be applicable to the NSTAR ion engine. Another three failure modes were added to the list of credible NSTAR failure mechanisms based on extrapolation of erosion characteristics from endurance tests which were suspended before failure and test experience with the NSTAR thruster.

Validation of the service life and quantification of the failure risk for the NSTAR ion engine is being accomplished through a combination of extended duration testing and probabilistic analyses of the credible failure modes. Probabilistic modeling techniques are needed to quantify the uncertainties in projected engine life due to allowable variations in the engine input parameters and any lack of knowledge regarding the behavior of model drivers.

The application of probabilistic analyses to two failure modes; accelerator grid structural failure due to charge-

exchange erosion, and screen grid structural failure due to sputter-erosion from discharge chamber ions, indicates that neither of these failure modes is likely to be a serious risk to the successful completion of the on-going NSTAR 8,000-hr test. Nor are these failure modes likely to prevent demonstration of the engine qual Life of 12,000-hrs. There is much additional work needed to evaluate the other 5 credible failure modes for the NSTAR thruster.

### Acknowledgments

The authors sincerely thank the substantial number of people at LeRC and JPL who have contributed to the testing and analysis of the NSTAR ion engine including, Mike Patterson, Jim Sovey, Roger Myers, John Hamley, Frank Curran, Mike Marcucci, Jack Stocky, Keith Goodfellow, Charles Garner, John Anderson, Al Owens, Bill Thogmartin and Bob Toomath.

The research described in this paper was conducted, in-part, at the Jet Propulsion Laboratory, under a contract with the National Aeronautics and Space Administration.

### References

1. Casani, E. K. and Lehman, D. H., "Deep Space One Memorandum of Agreement," Interoffice Memorandum, DSI-DHL-96-012, May 24, 1996, Internal JPL Document.
2. Patterson, M. J., et al., "2.3-kW Ion Thruster Wear Test," AIAA-95-2516, presented at the 31<sup>st</sup> AIAA/ASME/SAE/ASEE Joint Propulsion Conference, San Diego, CA, July 1995.
3. Polk, J. E., et al., "The Role of Analysis and Testing in the Service Life Assessment of Ion Engines," IEP-95-228, presented at the 24<sup>th</sup> International Electric Propulsion Conference, Moscow, Russia, Sept. 1995.
4. Polk, J. E., et al., "A 1000-Hour Wear Test of the NASA 30-cm Xenon Ion Engine," AIAA-96-2717, to be presented at the 32<sup>nd</sup> Joint Propulsion Conference, Lake Buena Vista, FL, July 1996.
5. Kaufman, H. R., "An Ion Rocket with an Electron-Bombardment Ion Source," NASA TN D-585, 1961.
6. Kaufman, H. R. and Reader, P. D., "Experimental Performance of an Ion Rocket Employing an Electron-Bombardment Ion Source," Paper 1374, American Rocket Society, Inc., 1960.
7. Reader, P. D., "Experimental Effects of Scaling on the Performance of Ion Rockets Employing Electron-Bombardment Ion Sources," Paper presented at the National IAS-ARS Joint meeting, Los Angeles, CA, 1961.
8. Nakanishi, S. and Pawlik, E. V., "Experimental Investigation of a 1.5-m-diam. Kaufman Thruster," *J. Spacecraft*, Vol. 5, No. 7, July 1968.

9. AIAA-67-81, 1967 -- micronewton cesium thruster reference.
10. Reader, P. D., "Investigation of a 10-Centimeter-Diameter Electron-Bombardment Ion Rocket," NASA TN D-1163, January 1962.
11. Kerslake, W. R., "Accelerator Grid Tests of an Electron-Bombardment Ion Rocket," NASA TN D-1168, February 1962.
12. Molitor, J. H., "Ion Propulsion Flight Experience, Life Tests and Reliability Estimates," AIAA-73-1256, AIAA/SAE Propulsion Conference, Las Vegas, Nevada, Nov. 1973.
13. Sohl, G., Reid, G. C. and Speiser, R. C., "Cesium Electron Bombardment Ion Engines," *J. Spacecraft*, Vol. 3, No. 7, July 1966.
14. Fosnight, V. V., et al., "Cesium Ion Engine System Life Test Results," *J. Spacecraft*, Vol. 5, No. 4, April 1968.
15. King, H. J., et al., "Electron-Bombardment Thrusters Using Liquid-Mercury Cathodes," *J. Spacecraft*, Vol. 4, No. 5, May 1967.
16. Kerslake, W. R. and Ignaczak, L. R., "Development and Flight History of SERT II Spacecraft," NASA TM 105636 (also AIAA-92-3516), July 1992.
17. Kerslake, W. R., "Status of SERT II Spacecraft and Ion Thruster - 1978," AIAA-78-662, presented at the 13<sup>th</sup> International Electric Propulsion Conference, San Diego, CA, April 1978.
18. Kerslake, W. R., Goldman, R. G. and Nieberding, W. C., "SERT II: Mission, Thruster Performance, and In-Flight Thrust Measurement," *J. Spacecraft*, Vol. 8, No. 3, March 1971.
19. Kerslake, W. R., et al., "Flight and Ground Performance of the SERT II Thruster," AIAA-70-1125, presented at the 8<sup>th</sup> Electric Propulsion Conference, Stanford, CA, August 1970.
20. Byers, D. C. and Staggs, J. E., "SERT II: Thruster System Ground Testing," *J. Spacecraft*, Vol. 7, No. 1, January 1970.
21. Stewart, D., "Life Testing of the UK T4A Thruster," AIAA-76-1023, presented at the AIAA International Electric Propulsion Conference, Key Biscayne, FL, Nov 1976.
22. Lathem, W. C., "1000-Hour Test of a Dual Grid, Electrostatic Beam Deflection Accelerator System on a 5-Centimeter-Diameter Kaufman Thruster," NASA TM X-67907, August 1971.
23. Nakanishi, S., "Durability Tests of a Five-Centimeter Diameter Ion Thruster System," AIAA-72-1151, presented at the AIAA/SAE 8<sup>th</sup> Joint Propulsion Specialist Conference, New Orleans, Louisiana, Nov. 1972.
24. Nakanishi, S. and Finke, R. C., "A 9700-Hour Durability Test of a Five Centimeter Diameter Ion Thruster," NASA TM X-68284, October 1973.
25. Lathem, W. C., "A Single-Axis Electrostatic Beam Deflection System for a 5-cm Diameter Ion Thruster," NASA TM X-68133, Sept. 1972.
26. Nakanishi, S. and Finke, R. C., "A 2000-Hour Durability Test of a 5-Centimeter Diameter Mercury Bombardment Ion Thruster," NASA TM X-68155, October 1972.
27. Lathem, W. C., "5000-Hour Test of a Grid-Translation Beam-Deflection System for a 5-cm Diameter Kaufman Thruster," NASA TM X-68185, January 1973.
28. Nakanishi, S., "A 15,000-Hour Cyclic Endurance Test of an 8-cm Diameter Mercury Bombardment Ion Thruster," AIAA-76-1022, presented at the International Electric Propulsion Conference, Key Biscayne, FL, November 1976.
29. Mantieniks, M. A. and Wintucky, E. G., "5200 Cycle Test of an 8-cm Diameter Hg Ion Thruster," NASA TM X-78860, April 1978.
30. Bechtel, R. T., "Effect of Neutralizer Position on Accelerator Wear for a 30-cm Diameter Ion Bombardment Thruster," NASA TM X-67926, September 1971.
31. Banks, et al., "8-cm Mercury Ion Thruster System Technology," NASA TM X-71611, October 1974.
32. Rawlin, V. K., Banks, B. A. and Byers, D. C., "Design, Fabrication, and Operation of Dished Accelerator Grids on a 30-cm Ion Thruster," AIAA-72-486, presented at the AIAA 9<sup>th</sup> Electric Propulsion Conference, Bethesda, MD, April 1972. Also, Rawlin, V. K., Banks, B. A. and Byers, D. C., "Dished Accelerator Grids on a 30-cm Ion Thruster," *J. Spacecraft*, Vol. 10, No. 1, January 1973.
33. Rawlin, V. K., "Studies of Dished Accelerator Grids for 30-cm Ion Thrusters," AIAA-73-1086, presented at the AIAA 10<sup>th</sup> Electric Propulsion Conference, Lake Tahoe, Nevada, October 1973.
34. Collett, C. R., "Endurance Testing of a 30-cm Kaufman Thruster," AIAA-73-1085, presented at the AIAA 10<sup>th</sup> Electric Propulsion Conference, Lake Tahoe, Nevada, October 1973.
35. Mantieniks, M. A. and Rawlin, V. K., "Studies of Internal Sputtering in a 30-cm Ion Thruster," AIAA-75-400, presented at the AIAA 11<sup>th</sup> Electric Propulsion Conference, New Orleans, LA, March 1975.
36. Collett, C. R., "A 7700-Hour Endurance Test of a 30-cm Kaufman Thruster," AIAA-75-366, presented at the AIAA 11<sup>th</sup> Electric Propulsion Conference, New Orleans, LA, March 1975.
37. Collett, C. R., et al., "Thruster Endurance Test," NASA CR-135011, May 1976.
38. Collett, C. R. and Bechtel, R. T., "An Endurance Test of a 900-Series 30-cm Engineering Model Ion Thruster," AIAA-76-1020, presented at the AIAA International Electric Propulsion Conference, Key Biscayne, FL, November 1976.

- 39 Bechtel, R. T., "Preliminary Results of the Mission Profile Life Test of a 30-cm Mercury Bombardment Thruster," AIAA-79-2079, presented at the AIAA/DGLR 14<sup>th</sup> International Electric Propulsion Conference, Princeton, NJ, October 1979.
- 40 James, E. L., and Bechtel, R. T., "Results of the Mission Profile Life Test First Test Segment: Thruster J1," AIAA-81-0716, presented at the AIAA/JSASS/DGLR 15<sup>th</sup> International Electric Propulsion Conference, Las Vegas, Nevada, April 1981.
- 41 Masek, T. D., "SEP Thrust Subsystem Development," JPL TR No. 32-1579, March 1973.
- 42 Bechtel, R. T., Truump, G. E., and James, E. J., "Results of the Mission Profile Life Test," AIAA-82-1905, presented at the AIAA/JSASS/DGLR 16<sup>th</sup> International Electric Propulsion Conference, New Orleans, LA, November 1982.
- 43 Beattie, J. R., Matossian, J. N., and Robson, R. R., "Status of Xenon Ion Propulsion Technology," AIAA-87-1003, presented at the 19<sup>th</sup> AIAA/DGLR/JSASS International Electric Propulsion Conference, Colorado Springs, CO, May 1987.
- 44 Francoise, D. R., Low, C. A., and Power, J. L., "Successful Completion of a Cyclic Ground Test of a Mercury Ion Auxiliary Propulsion System," NASA TM 101351 (also HEPC-88-035), presented at the 20<sup>th</sup> International Electric Propulsion Conference, Garmisch-Partenkirchen, West Germany, October 1988.
- 45 Dulgeroff, C. R., et al., "IAPS (8-cm) Ion Thruster Cyclic Endurance Test," HEPC-84-37, presented at the International Electric Propulsion Conference, Tokyo, Japan, May 1984.
- 46 Rawlin, V. K., "Internal Erosion Rates of a 10-kW Xenon Ion Thruster," AIAA-88-2912, presented at the 24<sup>th</sup> Joint Propulsion Conference, Boston, MA, July 1988 (also NASA TM 100954).
- 47 Patterson, M. J., and Verhey, T. R., "5-kW Xenon Ion Thruster Lifestest," NASA TM 103191, July 1990 (also AIAA-90-2543).
- 48 Brophy, J. R., Pless, L. C., and Garner, C. E., "Ion Engine Endurance Testing at High Background Pressures," AIAA-92-3205, presented at the AIAA/SAE/ASME/ASEE 28<sup>th</sup> Joint Propulsion Conference, Nashville, TN, July 1992.
- 49 Brophy, J. R., Polk, J. E., and Pless, L. C., "Test-to-Failure of a Two-Grid, 30-cm-dia. Ion Accelerator System," HEPC-93-173, presented at the 23<sup>rd</sup> International Electric Propulsion Conference, Seattle, WA, Sept. 1993.
- 50 Kitamura, S., et al., "1000 Hour Test of a 14-cm Diameter Ring-Cusp Ion Thruster," AIAA-90-2542, 1990.
- 51 Kitamura, S., Miyazaki, K., and Hayakawa, Y., "Cyclic Test of a 14-cm Diameter Ring-Cusp Xenon Ion Thruster," AIAA-92-3146, presented at the 28<sup>th</sup> Joint Propulsion Conference, Nashville, TN, July 1992.
- 52 Shimada, S., "Ion Thruster Endurance Test Using Development Model Thruster for ETS-VI," HEPC-93-109, presented at the 23<sup>rd</sup> International Electric Propulsion Conference, Seattle, WA, Sept. 1993.
- 53 Martin, A. R., et al., "Erosion Measurements for Two- and Three-Grid Ion Thruster Extraction Systems," HEPC-93-171, presented at the 23<sup>rd</sup> International Electric Propulsion Conference, Seattle, WA, Sept. 1993.
- 54 Kerlake, W. R., "Cathode Durability in the Mercury Electron-Bombardment Ion Thruster," AIAA-64-683, presented at the 4<sup>th</sup> Electric Propulsion Conference, Philadelphia, PA, August 1964.
- 55 Rawlin, V. K., and Kerlake, W. R., "SERI II Durability of the Hollow Cathode and Future Applications of Hollow Cathodes," *J. Spacecraft*, Vol. 7, No. 1, Jan. 1970.
- 56 Mantionicks, M. A., "Mercury Ion Thruster Component Testing," AIAA-79-2116, 1979.
- 57 Verhey, T., Lewis Research Center, March 1990, personal communication.
- 58 Patterson, M. J. NASA Lewis Research Center, Feb. 1990, personal communication.
- 59 Polk, J. E., Brophy, J. R., and Wang, J., "Spatial and Temporal Distribution of Ion Engine Accelerator Grid Erosion," AIAA-95-2924, presented at the 31<sup>st</sup> Joint Propulsion Conference, July 1995.
- 60 Rawlin, V. K., "Erosion Characteristics of Two-Grid Ion Accelerating Systems," HEPC-93-175, presented at the 23<sup>rd</sup> International Electric Propulsion Conference, Sept. 1993.
- 61 Fox, E., personal communication, December 1995.
- 62 Aztec Box V2.41, Aztec Associates, Inc., copyright © 1995.
- 63 Moore, N., Ebbeler, D., and Creager, M., "Probabilistic Service Life Assessment," in Reliability Technology, 1992, Vol. AD-28, American Society of Mechanical Engineers, 1992. ISBN 0-7918-1095-X.
- 64 Moore, et al., "An Improved Approach for Flight Readiness Assessment: Methodology for Failure Risk Assessment and Application Examples," JPL 92-15, Jet Propulsion Laboratory, California Institute of Technology, Pasadena, CA, 1992.
- 65 Rosenberg, D., and Wehner, G. K., "Sputtering Yields for Low Energy He<sup>+</sup>, Kr<sup>+</sup>, and Xe<sup>+</sup> Ion Bombardment," *Journal of Applied Physics*, Vol. 33, No. 5, May 1962.
- 66 Rawlin, V. K., "Screen grid wear at low flow and high beam current conditions," NSTAR Memorandum, April 17, 1996, Lewis Research Center document.

Table 1 Ion Thruster Endurance Tests

Thruster	Year	Hours	Prop.	$J_{eff}$ (A)	$I_{eff}$ (V)	$J_{eff}/J_{th}$ (%)	$I_{eff}$ (V)	$I_{eff}$ (V)	Comments	
5 cm Thrusters	• SIT-5: Electrostatic thrust vectoring grids [22]	1972	Hg	0.025	1200	<1	-1200	40	Groove erosion from neut. Erosion by direct ion imp. Warping of accel grid strips.	
	• SIT-5: Translating screen grid [23,26]	1972	Hg	0.025	1000	<0.5	-1000	37-40	1 <sup>st</sup> 2030 hrs with translating screen grid. Little accel erosion. 20,000-hr projected grid life. No "pits & grooves" pattern. 10 <sup>th</sup> thrust vectoring	
	• SIT-5: Electrostatic thrust vectoring grids [23,24]	1973	Hg	0.025	1300	N/A	-900	38-40	Last 7692 hrs with electrostatic thrust vectoring grids on same discharge chamber. Three grid shorts cleared by "zapping". Accel grid failure terminated the test due to flakes on screen grid. Significant neut. on/off plate erosion.	
	• SIT-5: Single axis electro-static thrust vector [25]	1972	Hg	0.025	1400	0.18	-500	N/A	Projected grid lifetime of 10,000-hrs with minor mods.	
8 cm Thrusters	• SIT-5: Translating screen grid [27]	1973	Hg	0.025	1000	N/A	-1000	N/A	Continuation of 2023 hr test above for a total of 5000-hrs on the grids. Last 3-khrs with no beam deflection. No flakes. Projected 20,000-hr grid life.	
	8 cm Thrusters									
	• A1S-1 [12]	1970	465	CS	N/A	N/A	N/A	N/A	Projected lifetime 10,000 to 20,000 hrs	
	• A1S-1 [12]	1972	750	CS	N/A	N/A	N/A	N/A		
	• A1S-1 [12]	1973	1100	CS	N/A	N/A	N/A	N/A		
	• 8-cm Lab model [31]	1974	200	Hg	0.231	1393	0.27	-700	61.6	Accelerated discharge chamber erosion test (intentionally high $I_{eff}$ )
	• 8-cm Lab model [31]	1974	1000	Hg	N/A	N/A	N/A	N/A	Ion machined accelerator grid	
	• 8-cm Lab model [28]	1976	15,040	Hg	0.072	1240	0.47	-500	37	460 on/off cycles. Baffle replaced at 1156 hrs. >200 V decrease in electron-backstreaming margin. Considerable erosion of the accel grid. No change in thruster performance.
	• 8-cm EMIT [29]	1978	1300	Hg	0.072	1220	0.19	-300	40	5200 on/off cycles. No change in screen or accel grid thickness. Chamfering on the upstream side of the accel grid.
	• 8-cm IAPS [45]	1981	9189	Hg	0.072	1200	0.35	-290	38	Significant neut. erosion. Isolator braze joint failure. Charge-exchange through pits in accel grid. Grid short from accel material deposited on screen grid developed in post test handling. Little change in thruster performance.

Thruster	Year	Hours	Prop.	$J_B$ (A)	$V_B$ (V)	$J_A/J_B$ (%)	$V_A$ (V)	$V_D$ (V)	Comments
• 8-cm IAPS [44]	1988	7057	Hg	0.071	1208	0.44 to 0.69	-303	38	2557 on/off cycles. Neutralizer degradation with time. Substantial accel. grid erosion, but no through pits. Accel. grid aperture enlargement (17% increase in open area fraction). No loose flakes in the discharge chamber.
<b>10 cm Thrusters</b>									
• 1st Kaufman Thruster [10,11]	1962	150	Hg	0.20	2500	1	-1000	50	Accel. grid mass loss rate 15.3 g/chr. Projected accel. grid life of 1000 hrs. Beam flatness parameter 0.40.
• UK T4A [21]	1976	2315	Hg	0.16	N/A	0.29	-190	40	In 2 tests with different cathodes. Grid life projected at > 30,000 hrs. Flakes appeared at 701 hrs.
• UK T5 Mark 3 [53]	1993	500	Xe	0.457	1100	0.38	-225	38.2	Three-grid with negative decel. grid can reduce accel. grid erosion.
		500	Xe	0.457	1100	0.38	-225	38.2	
<b>12-cm Thrusters</b>									
• DF-1 [13,14]	1965	2610	Cs	0.440	3700	1.1	-500	N/A	Projected grid life of > 20,000 hrs.
• DF-2 [13,14]	1966	3670	Cs	0.439	3700	1.3	-380	N/A	
• DF-3 [13,14]	1966	8150	Cs	0.434	3650	1.8	-320	N/A	Cathode heater failure. Neutralizer clogging
• TRS BBM [52]	1990	9100	Xe	0.500		1		37	Severe accel. grid erosion. Switch to 3-grid system. Sputter-resistant coatings. Mesh for flake control
• TRS DM #1 [52]	1991	7200	Xe	0.500		1		37	Added neutralizer shield. Expanded mesh for flake control. Severe screen grid erosion. Significant accel. grid erosion
• TRS DM #2 [52]	1991	7100	Xe	0.500		1		37	
• TRS EM #1 [52]	1992	6200	Xe						2278 on/off cycles
• TRS EM #2 [52]	1992	5981	Xe						2305 on/off cycles. Expanded mesh
• TRS EM #3 [52]	1992	6873	Xe						2387 on/off cycles. for flake control
• TRS EM #4 [52]	1992	8129	Xe						3233 on/off cycles
• TRS PM #1 [52]	1993	4568	Xe						Expanded mesh for flake control
• TRS PM #2 [52]	1993	4534	Xe						
<b>14 cm Thrusters</b>									
• NAL 14-cm Lab model [50]	1990	1000	Xe						
• NAL 14-cm Lab model [51]	1992	1859	Xe	0.474	1000	N/A	-800	35.2	613 on/off cycles. Neut. degradation. Substantial cathode erosion. Discharge chamber flakes
<b>15 cm Thrusters</b>									
• SERT II Lab thruster 1 [12]	1969	1800	Hg	N/A	N/A	N/A	N/A	N/A	In 13 tests of shields to prevent "groove" erosion
• SERT II Lab thruster 2 [12,20]	1969	3300	Hg	0.252	3000	0.48	-2000	37	In 2 tests. Neut. erosion at high $V_{N/Z}$ . Cath. orifice dia. increase.
• SERT II Prototype (P-3) [12]	1969	1000	Hg	N/A	N/A	N/A	N/A	N/A	Planned 1000-hr test
• SERT II Prototype (P-5) [12]	1969	4729	Hg	N/A	N/A	N/A	N/A	N/A	In 3 tests. frozen Hg line. replaced main cath. with flight design
• SERT II Prototype (P-20) [12]	1970	779	Hg						Arcing internal to PPU

Thruster	Year	Hours	Prop.	$J_H$ (A)	$I_H$ (V)	$J_A/J_H$ (%)	$V_A$ (V)	$I_D$ (V)	Comments
• SERT II Test M (P-20) [12,16,18,19]	1970	2750 4037	Hg	0.255 0.200	3190 3230	0.48 0.8	-1660 -1680	37.4 37.5	Propellant tank emptied. Last 4037 hrs at 80° power due to isolator/vaporizer problem
• SERT II Test T (P-10) [12,16,18,19]	1970	5169	Hg	0.253	3130	1.0	-1610	36.4	Voluntarily terminated. Loss of vacuum at 1400 and 3190 hrs, thruster cleaned of sputter-deposited material each time.
• SERT II Flight #1 [16-18]	1970	3781	Hg	0.25	3000	0.6	-1550	37	Unclearable grid short
• SERT II Flight #2 [16-18]	1970	2011 664	Hg	0.25 0.085	3000 3000	0.6 1.2	-1550 -1500	37 42	Grid short. Short cleared in 1974. Impinged new propellant tank
• JPL LM Cath. [14]	1967	4009	Hg	0.60	6100	0.48	N/A	N/A	Projected accel grid life of 10,500 hrs. End of life is determined by bridge erosion.
• JPL 20-cm [12,41]	1971	1500	Hg	N/A	N/A	N/A	N/A	N/A	2 thrusters run simultaneously. One cathode failure.
• 25-cm XIPS [43]	1985	4350	Xe	1.45	750	0.34	-300	28	3850 on/off cycles. Early cathode erosion resulted in cathode replacement after a few hundred hrs. Accel grid aperture enlargement. Grid shorts cleared by "zapping"
<b>30 cm Thrusters</b>									
• 30-cm Lab Model [30]	1971	280	Hg	1.5	1000	2.3	-500	N/A	Confirm the effect of neut. orientation on accel grid erosion.
• 30-cm Lab Model [32]	1972	1365	Hg	2.5	1000	0.32	-500	40	Last 700 hrs at the operating point shown. Extrapolated time to failure > 10,000 hrs.
• 30-cm Lab Model [33]	1973	1552	Hg	2.0 to 2.5	N/A	0.2 to 0.3	-500	N/A	No erosion from neutralizer ions.
• 30-cm Lab Model [33]	1973	1580	Hg	2.0 to 2.5	N/A	0.2 to 0.3	-500	N/A	No erosion from neutralizer ions. Accel. pit depth < 0.01 mm.
• 30-cm Lab Model [34]	1973	500	Hg	1.5	1330	0.33	-600	37	Flat grids with center support
• 30-cm Lab Model [34]	1973	500	Hg	1.5	1330	0.33	-500	37	Distal grids. Cathode heater problem.
• 30-cm Lab Model [34]	1973	1100	Hg	1.5	1330	0.33	-600	37	Planned for 6000 hrs. Catastrophic loss of vacuum at 1100 hrs with engine on. Lots of back-sputtered SS from vacuum tank due to beam divergence. Cathode isolator degradation with time.
• 30-cm Lab Model [35]	1975	1872	Hg	1.5 to 2.0	1100	N/A	-500	33 to 40	19 test segments. Screen grid gained 1.9 g. accel. grid lost 3.3 g (1.76 g/Khr)

Thruster	Year	Hours	Prop.	$J_B$ (A)	$V_B$ (V)	$J_A J_B$ (% $\phi$ )	$V_A$ (V)	$V_D$ (V)	Comments
• 30-cm 701 EMT [36,37]	1975	10,000	Hg	1.7 to 0.5	1100	0.2	-500	37	Beam current started at 1.5 A, was changed to 1.75 A, then 1.5 A, 1.0 A and finally 0.5 A. Flakes on screen grid at 4530 hrs. Hole in baffle at 5845 hrs. Discharge chamber failure at 7300 hrs (could no longer maintain full beam current). Grid shorts cleared by "zapping." Grids were no longer functional after the test. Cathode and neut. had little erosion.
• 30-cm 901 EMT [38]	1976	4165	Hg	2.0	1100	N/A	-300	35	Planned for 10,000 hrs. Terminated at 4165 hrs by a shorted wire under the ground screen. Flakes in the discharge chamber after 4165 hrs. Cathode orifice in excellent condition. Higher than expected screen grid erosion (370 $\mu$ m eroded to 240 $\mu$ m). Sliver of material on screen grid at 2670 hrs. $\phi$ 18 $\mu$ m screen grid erosion. No cathode erosion, slight neut. orifice chamfering. Engine life projected to be consistent with 15,000 hrs.
• 30-cm J-1 EMT [39,40]	1981	4263	Hg	2.0	1100	0.37	-300	32	Planned for 15,000 hrs. Contract terminated
• 30-cm J2 EMT [42]	1982	819	Hg	2.0	1100	0.37	-300	32	Planned for 15,000 hrs. Cathode propellant isolator failure.
• 30-cm J3 EMT [42]	1982	2785	Hg	2.0	1100	0.37	-300	32	Planned for 4,000 hrs. Severe grid arcing.
• 30-cm J4 EMT [42]	1982	104	Hg	2.0	1100	0.37	-300	32	Planned for 4,000 hrs at min. power. Voluntarily terminated.
• 30-cm J5 EMT [42]	1982	5070	Hg	0.75	600	0.15	-285	32	Planned for 4,000 hrs. Cathode propellant isolator failure.
• 30-cm J6 EMT [42]	1982	390	Hg	2.0	1100	0.37	-300	32	Planned for 4,000 hrs. TC short
• 30-cm J7 EMT [42]	1982	336 408 689	Hg Hg Hg	2.0	1100	0.37	-300	32	Planned for 400 hrs. End of test. Planned for 700 hrs. Failing main propellant isolator
• 30-cm J-Series [46]	1988	500	Xe	5.0			-500		Wear test at 10-kW. J-Series thruster design not suitable to long life at 10 kW due to baffle erosion.
• 30-cm Lab Model Ring-Cusp [47]	1990	900	Xe	3.2					5.5 kW wear test. Accel. through pits. Cathode ignitor erosion. Cathode orifice plate erosion. No flakes. Little screen grid erosion. Projected accel. grid life of 11,000 hrs
• 30-cm J-Series [48]	1992	900	Ar	3.5	1550	0.35	-210	45	Negative decel. grid used to protect the accel. grid. Little accel. grid erosion at 6.0 kW.
• 30-cm J-Series [49]	1993	633	Kr	2.8	1050	1.25	-500	43	Intentional test to failure of the accelerator grid. Intentionally enhanced accel grid erosion to shorten the test. End of test was due to grid shorting.

Thruster	Year	Hours	Prop.	$J_B$ (A)	$V_B$ (V)	$J_A/J_B$ (%)	$V_A$ (V)	$V_D$ (V)	Comments
• 30-cm NSTAR EMT1 [2]	1995	2150	Xe	1.76	1100	0.48	-180	26.8	Propellant isolator failure. High screen grid erosion, discharge chamber flakes. High cathode erosion. No neut. erosion. Acceptable accel. grid erosion. Projected accel. grid life of 21,500 hrs.
• 30-cm NSTAR EMT1b [4]	1995	1024	Xe	1.76	1100	0.48	-180	24.5	No cathode erosion. No screen grid erosion. No discharge chamber flakes. Acceptable accel. grid erosion.